THE JOURNAL OF BIOLOGICAL CHEMISTRY VOL. 287, NO. 8, pp. 5278–5289, February 17, 2012

Macro Histone H2A1.2 (MacroH2A1) Protein Suppresses Mitotic Kinase VRK1 during Interphase*[S]

Received for publication, July 11, 2011, and in revised form, December 6, 2011 Published, JBC Papers in Press, December 22, 2011, DOI 10.1074/jbc.M111.281709

Wanil Kim[‡], Goutam Chakraborty[§], Sangjune Kim[‡], Joon Shin[§], Choon-Ho Park[‡], Min-Woo Jeong[‡], Nagakumar Bharatham[§], Ho Sup Yoon[§], and Kyong-Tai Kim[‡¶1]

From the [‡]Department of Life Science, Division of Molecular and Life Science, and [¶]Division of Integrative Biosciences and Biotechnology, Pohang University of Science and Technology, Pohang 790-784, Republic of Korea and the [§]School of Biological Sciences, Nanyang Technological University, Singapore 637551

Background: VRK1 phosphorylates mitotic histone H3 at Thr-3 and Ser-10, but its negative regulator was not elucidated during interphase.
Results: The macrodomain of macroH2A1 interacts with VRK1, and this suppresses enzymatic activity of VRK1 during interphase.
Conclusion: Specific binding between VRK1 and macroH2A1 is required to regulate the cell cycle-dependent histone H3 phosphorylation.
Significance: Understanding epigenetic regulation of histone H3 during the cell cycle is important in cancer development.

VRK1-mediated phosphorylation of histone H3 should be restricted in mitosis for consistent cell cycling, and defects in this process trigger cellular catastrophe. However, an interphasic regulator against VRK1 has not been actually investigated so far. Here, we show that the histone variant macrodomain-containing histone H2A1.2 functions as a suppressor against VRK1 during interphase. The level of macroH2A1.2 was markedly reduced in the mitotic phase, and the macroH2A1.2-mediated inhibition of histone H3 phosphorylation occurred mainly during interphase. We also found direct interaction and binding features between VRK1 and macroH2A1.2 by NMR spectroscopy. Hence, our findings might provide valuable insight into the underlying molecular mechanism regarding an epigenetic regulation of histone H3 during the cell cycle.

The cell cycle is exquisitely regulated by numerous factors, and unregulated permanent cell proliferation is frequently associated with the malfunction of essential factors involved in the cell cycle. Among the diverse key players, several protein kinases play the most critical roles in the proper and well regulated progression of the cell cycle. In this regard, vaccinia-related kinase 1 (VRK1) has recently been highlighted as a novel cell cycle regulator. VRK1 is the eukaryotic counterpart of the *Vaccinia* virus B1R kinase that is essential for viral replication (1). To date, several substrates for VRK1 have been characterized, most of which are related to cell survival and proliferation. VRK1 phosphorylates Thr-18 of p53 and thereby stabilizes p53 (2–4). Phosphorylated p53 targets VRK1 to the endosome-lysosome degradation pathway, creating an auto-regulatory loop (5, 6). VRK1 can also phosphorylate activating transcription factor 2 and c-Jun by its interaction with JNK (7, 8). During cell cycle progression, VRK1 has been shown to phosphorylate barrier-to-autointegration factor (BAF),[2] which is believed to compact DNA (9–11), and it has also been shown to be involved in promoting the transcription of proliferation-related proteins such as retinoblastoma, cyclin-dependent kinase-2, and survivin (12). Additionally, VRK1 can increase cyclin D1 expression via the phosphorylation of the cAMP-response element-binding protein and has a major role in the G_1/S transition (13, 14). More recently, VRK1 has been demonstrated to play crucial roles in germ cell development (15–17).

Chromatin condensation, which facilitates the assembly and subsequent segregation of chromosomes into two daughter cells, is required for the initiation of mitosis. The phosphorylation of histones is one of the prominent signals prior to chromatin condensation. In mammals, phosphorylation on Ser-10 and Thr-3 on histone H3, by Aurora kinase B and haspin, respectively, are considered the most important events for chromosome condensation and chromosome assembly (18, 19). We have shown that VRK1 phosphorylates Thr-3 and Ser-10 of histone H3 (20).

The mitotic phosphorylation of histones appears at the late G_2 and M phases to enable successful cell division, and irregular phosphorylation of histones triggers severe cellular catastrophe (18). Therefore, accurate spatiotemporal regulation of mitotic histone kinases is essential. As mentioned earlier, the mitotic phosphorylation of histone H3 Thr-3 and Ser-10 requires haspin and Aurora B kinase, in addition to VRK1 (18). The level of expression of Aurora kinase B is tightly coordinated with histone H3 phosphorylation during the G_2/M transition (19); this mode of expression permits the mitosis-specific phosphorylation of histone H3. However, the expression of haspin kinase

* This work was supported by National Research Foundation of Korea Grants 20100030089, 20100002146, and 20100019706, the Brain Korea 21 Program, the World Class University Program Grant R31-10105, and the Regional Core Research Program/Anti-aging and Well Being Research Center funded by the Korean Ministry of Education, Science, and Technology.
[S] This article contains supplemental Figs. 1–7.
[1] To whom correspondence should be addressed. Tel.: 82-54-279-2297; Fax: 82-54-279-2199; E-mail: ktk@postech.ac.kr.

[2] The abbreviations used are: BAF, barrier-to-autointegration factor; macroH2A1; macro histone H2A1.2; EGFP, enhanced green fluorescent protein; BrdU, bromodeoxyuridine; HSQC, heteronuclear single quantum correlation.

remains steady throughout the cell cycle. However, haspin localizes to the centromere, centrosomes, and spindle during the mitotic phase, and specific cellular factors such as Aurora kinase B and polo-like kinase1 seem to have an important role in this selective distribution and activation (18, 21). The amount of VRK1 protein increases in the late G_2 and M phases and then decreases at the end of anaphase (20). However, VRK1 is still maintained at significant levels during interphase and plays some important roles (13, 14). Therefore, the tail of histone H3 must be protected from VRK1 by specific cellular factors during interphase and exposed to VRK1 only at the late G_2 and M phases, because these proteins always colocalize in the nucleus and maintain their expression levels throughout the cell cycle. For the proper control of the cell cycle, the enzymatic activity of VRK1 in histone H3 phosphorylation should be restricted during interphase. However, little is known about the mechanism by which VRK1 activity is suppressed in the nucleus during interphase.

Here, we present the macroH2A1.2 protein (hereafter referred as macroH2A1) as a potential suppressor of VRK1 action during interphase. MacroH2A1 is a core histone variant containing a histone domain and a large non-histone part called the macrodomain (22). MacroH2A1 is primarily known to be incorporated into nucleosomes and is related to X chromosome inactivation, with a strong tendency to localize in the inactivated X chromosome (23). According to recent reports, there are also several lines of evidence that macroH2A1 is associated with general silencing of gene expression. The silencing mechanism of nucleosome-charged macroH2A1 appears to be associated with the repulsion of transcription factors from promoter/enhancer regions (24, 25). Recent studies have also revealed that macroH2A1 shows cell cycle-dependent changes in localization (26) and post-translational modification (27). However, the relationship between macroH2A1 and cell cycle regulation is not known. We present evidence that macroH2A1 binds to VRK1 and sequesters it from histone H3 during interphase of the cell cycle.

EXPERIMENTAL PROCEDURES

Cell Culture and Transfection—HeLa and HEK293A were maintained in Dulbecco's modified Eagle's medium (DMEM) containing 10% fetal bovine serum and 1% penicillin/streptomycin in a humidified 5% CO_2 incubator at 37 °C. A549 and HCT116 were fed with RPMI 1640 medium. Transient transfection was performed by using METAFECTENE (Biontex, Germany) for 24 h according to the manufacturer's instruction. Transient transfection was also performed by using a microporator MP-100 (Invitrogen) according to manufacturer's instruction (1300 V, 20 ms, number 2 for A549).

Plasmids and siRNAs—To generate macroH2A1.2 (macroH2A1) expression construct, full-length macroH2A1 was amplified by PCR from HeLa cells. For mammalian expression, DNA fragment coding for macroH2A1 was cloned into pcDNA3.1 containing hemagglutinin (HA) sequences and pFLAG-CMV2 (Sigma). For bacterial expression of macroH2A1, the DNA fragment was cloned into pGEX-4T-3 (GE Healthcare) and pPROEX-HTa (Invitrogen). pFLAG-CMV2-VRK1 and pGEX-VRK1 were generated as described previously (13, 28). VRK1 was also cloned into pDsRed1-monomer-N1 vector (Clontech). The DNA fragment coding macrodomain (residues 180–360) of macroH2A1 and C-terminal truncated form of macroH2A1 (macroH2A1–350aa) was PCR-amplified using pGEX-4T3-macroH2A1 as template, and the amplified DNA fragment was cloned into pETSUMO vector (LIFE Sensors) and into pcDNA3.1 containing HA. To generate His-tagged recombinant BAF, full-length BAF was amplified by using RT-PCR amplified from HeLa cells. BAF was cloned into pPROEX-HTa (Invitrogen). To generate EGFP-conjugated BAF, pPROEX-HTa-BAF was used as template, and the amplified DNA fragment was cloned into pEGFP-C1 (Clontech). Expression constructs for the haspin and Aurora kinase B were kind gifts from J. M. Higgins (Harvard Medical School) and C. W. Lee (Sungkyunkwan University, Korea), respectively. All kinds of siRNAs against macroH2A1, Aurora kinase B, and haspin were synthesized (Bioneer, Korea). RNA interference against macroH2A1 was performed with a mixture of three selected siRNAs for coding sequence (supplemental Fig. S7) or one selected siRNA for 3′-UTR. Sequences are listed as follows: si-macroH2A1.#1, 5′-UGG AAU ACC UGA CAG CGG A-3′; si-macroH2A1.#2, 5′-CCG AGU UGC UAG CGA AGA A-3′; si-macroH2A1.#3, 5′-GUG AUC CAC UGU AAU AGU C-3′; and si-macroH2A1.3′-UTR 5′-TTA ATA AGG CAA AGC AGA A-3′.

Antibodies—VRK1 antiserum was generated in rabbit by using full-length recombinant VRK1 protein (supplemental Fig. S6). The other antibodies were purchased as follows: anti-FLAG from Sigma; anti-HA from Roche Applied Science; anti-macroH2A1 from Upstate, anti-histone H3 from Cell Signaling; anti-GAPDH from Santa Cruz Biotechnology; anti-histone H3 phospho-Thr-3 from Cell Signaling; anti-histone H3 phospho-Ser-10 from Abcam; anti-Lamin A/C from Cell Signaling; anti-cyclin B1 from Santa Cruz Biotechnology; anti-haspin from Bethyl Laboratories; anti-Aurora kinase B from BD Biosciences; anti-phospho-cdc25C (Thr-48) from Cell Signaling.

Immunoblot Analysis—After washing two times with PBS, cells were harvested and then lysed with lysis buffer (20 mM Tris (pH 7.5), 150 mM NaCl, 1 mM EDTA, 1 mM EGTA, 1% Triton X-100, 2.5 mM sodium pyrophosphate, 1 mM β-glycerophosphate, 10 mM Na_3VO_4, 1 μg/ml leupeptin, 1 μg/ml aprotinin, 1 mM PMSF). Equal amounts of lysates were separated by SDS-PAGE and transferred to nitrocellulose membrane. Membrane was blocked with TTBS (150 mM NaCl, 10 mM Tris-HCl (pH 7.4), 0.05% Tween 20) containing 5% skim milk for 30 min and incubated with selected primary antibodies overnight. Each protein was detected with HRP-conjugated secondary antibodies and ECL detection system.

Protein Expression and Purification—Escherichia coli BL21(DE3) pLysS cells (Novagen) transformed with plasmids coding for His-macroH2A1, GST-macroH2A1, GST-VRK1, and His-VRK1 were grown to A_{600} = 0.4–0.7, and proteins were induced for 20 h at 18 °C with 1.0 mM isopropyl β-D-1-thiogalactopyranoside. For the purification of His-macroH2A1 and His-VRK1, cells were harvested, resuspended in a lysis buffer (20 mM phosphate buffer (pH 7.8), 500 mM NaCl, 1 mM PMSF), and purified on a Ni^{2+}-nitrilotriacetic acid-agarose column (Invitrogen). The eluted proteins were concentrated and

further purified on a Superdex S-200 column (GE Healthcare) pre-equilibrated with a buffer containing 25 mM Tris-HCl buffer (pH 8.0), 1 mM DTT, and 50 mM NaCl. For purification of GST-macroH2A1 and GST-VRK1, bacterial pellets were resuspended in a lysis buffer (50 mM Tris-Cl (pH 8.0), 25 mM NaCl, 2 mM EDTA). The suspended cells were further lysed by sonication, clarified by centrifugation, and purified on a glutathione-Sepharose 4B column (GE Healthcare). BAF was purified under denaturing conditions. The inclusion bodies were resuspended in 6 M guanidine HCl, 2 mM β-mercaptoethanol, 150 mM KCl, 5 mM imidazole, 20 mM HEPES (pH 7.6), and 0.1 mM EDTA for 2 h at RT. After clarification by centrifugation, the supernatant was applied to Ni^{2+}-nitrilotriacetic acid-agarose for 12 h at 4 °C, followed by washing and re-folding with PBS.

In Vitro Kinase Assay—Kinase assays were performed with 500 ng of VRK1 and 100 ng to 2 μg of macroH2A1. 5 μg of core histone complex (gift from K. J. Kim, X-ray Research Group, POSTECH, Korea) and 500 ng of BAF were used as substrates for VRK1. All kinase reactions in the presence of substrates were performed as described previously (2).

Cell Cycle Synchronization and Flow Cytometry—Before synchronization, cells were prepared to 70% confluency. G_1 arrest was achieved by treating 500 μM mimosine (Sigma), in S arrest by treating 1 mM hydroxyurea (Sigma), in G_2-arrest by treating 500 μM of cisplatin (Sigma), and in M-arrest by treating 50 ng/ml of nocodazole (Sigma) for 16 h. Aliquots were analyzed by flow cytometry, and the remaining cells were used for preparing cell lysates. For flow cytometry, cells were fixed with 70% ethanol with 0.4% Tween 20. After centrifugation, cellular DNA was stained with 50 μg/ml propidium iodide (Fluka) and 100 μg/ml RNase A (Sigma) in PBS. After 1 h of incubation at room temperature, samples containing 10,000 cells were analyzed on a FACSCalibur system (BD Biosciences). Staining of phosphohistone H3 Ser-10 (from Abcam) was performed according to the manufacturer's instruction. BrdU-incorporated cells were analyzed using allophycocyanin-BrdU Flow kit assay system (Pharmingen) according to the manufacturer's instruction.

Pulldown Assay—Immunoprecipitation was performed with 1 μg of antibodies and 30 μl of protein A-Sepharose slurry (GE Healthcare) in cell lysis buffer (20 mM Tris (pH 7.5), 150 mM NaCl, 1 mM EDTA, 1 mM EGTA, 1% Triton X-100, 2.5 mM sodium pyrophosphate, 1 mM β-glycerophosphate, 10 mM Na_3VO_4, 1 μg/ml leupeptin, 1 μg/ml aprotinin, 1 mM PMSF) at 4 °C for 12 h. GST pulldown assay was performed with 10 μg of GST-fused protein and 30 μl of glutathione-Sepharose 4B (GE Healthcare) in cell lysis buffer. 1 mg of total cell lysate or indicated amount of recombinant protein was used for each reaction. After washing five times, general Western blot analysis was performed.

RESULTS

Association and Colocalization of MacroH2A1 and VRK1—VRK1 is a novel mitotic Ser/Thr kinase and its detailed molecular mechanism is yet unknown. To delineate the physiological role of VRK1 and its regulatory mechanism during the cell cycle transition, we attempted to identify binding partners of VRK1. To this end, we prepared GST-fused recombinant VRK1 protein as described previously (20). After incubation with total lysates from HeLa cells, proteins associating with GST-VRK1 were immunoprecipitated. By this approach, we identified macroH2A1 as a newly identified binding partner of VRK1 as determined by MALDI-TOF analysis (Fig. 1*A*). The core histone complex was also pulled down in this experiment, consistent with our previous observations (20). Purified recombinant proteins were prepared and immunoprecipitated to confirm the interaction between VRK1 and macroH2A1 (Fig. 1, *B* and *C*). Coimmunoprecipitation was also performed to confirm the specificity of the interaction between the purified macroH2A1 and VRK1 proteins and not with VRK2 and VRK3 (Fig. 1*D*). We also visualized the cellular colocalization of VRK1 and macroH2A1 by fluorescence microscopy (Fig. 1*E*); this suggests that VRK1 and macroH2A1 exist in the same partition and may therefore have a chance to interact.

Fluctuation of MacroH2A1 Levels during Cell Cycle—Even though VRK1 exhibits a dynamic pattern of expression throughout the cell cycle, it has a fairly stable level of expression and is localized in the nucleus during interphase (14, 20). However, histones are not significantly phosphorylated during interphase, despite the expression and colocalization of VRK1. This prompted us to examine whether the newly discovered interacting partner, macroH2A1, modulates VRK1 activity during interphase. Interestingly, macroH2A1 was previously reported to exhibit cell cycle-dependent localization in the chromatin of the X chromosome (26). However, fluctuations in the nucleosomal concentration of macroH2A1 during the cell cycle, and its biological significance, remain uncharacterized. Therefore, we initially attempted to measure macroH2A1 levels in nucleosomes throughout the cell cycle.

To accomplish this, A549 human lung carcinoma cells were treated with mimosine to induce G_1 arrest, hydroxyurea to induce S arrest, and nocodazole to induce G_2/M arrest (Fig. 2*A*). In each case, the chromatin fraction was separated from the cytoplasm and nucleoplasm and analyzed for macroH2A1 expression (Fig. 2*B*). Interestingly, the levels of macroH2A1 were significantly different in the G_1 and G_2/M phases, with the macroH2A1 level in the G_2/M phase decreasing to less than 50% of that seen in the G_1 phase (Fig. 2, *B* and *C*); simultaneously, the phosphorylation of histone H3 at Ser-10 increased dramatically. To examine whether the finding was specific to a particular cell line, we tested HCT116 human colorectal cancer cells and obtained results similar to those seen in A549 cells (supplemental Fig. S1), suggesting that this finding is not cell type-specific. This led us to speculate that fluctuations in macroH2A1 expression in the different cell cycle phases might be linked to the modulation of VRK1 activity and to histone H3 phosphorylation. Thus, to analyze time-dependent changes in the expression of macroH2A1, we treated cells with nocodazole and performed a mitotic shake-off experiment (supplemental Fig. S2). Our results show that the level of macroH2A1 increased from the releasing point (prometa phase). To inspect changes in the cellular levels of macroH2A1, we measured the relative amounts of macroH2A1 using immunofluorescence (Fig. 2*D*), and we found that chromatins in the mitotic phases (prophase, metaphase, and anaphase) had relatively low amounts of macroH2A1 compared with the amounts seen in interphase chromatins, indicating that the presence of mitotic

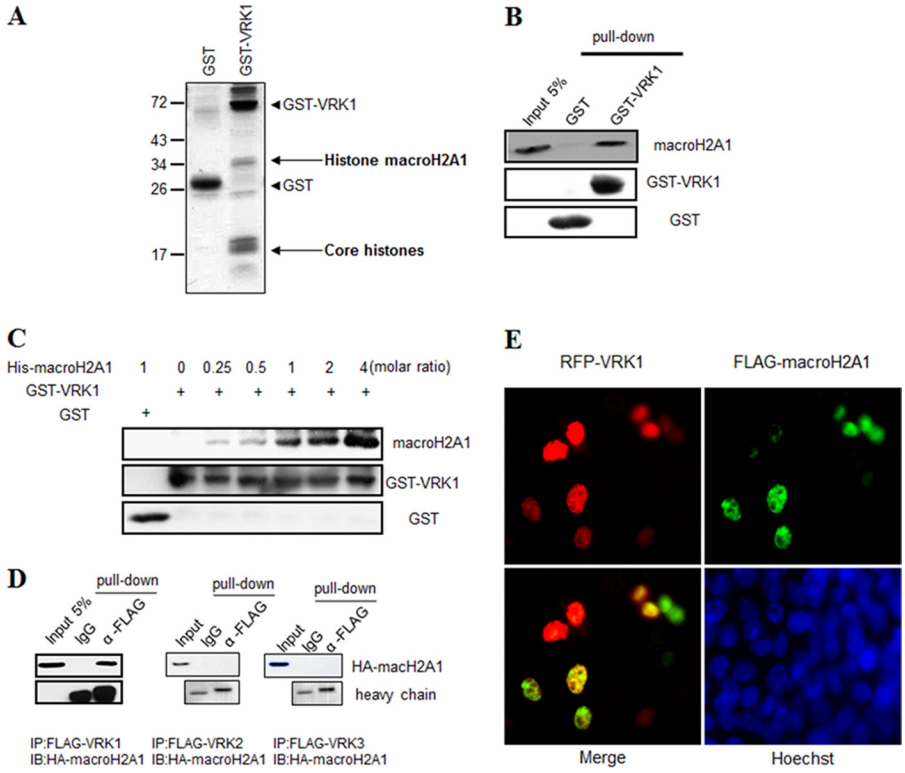

FIGURE 1. **Association and colocalization of macroH2A1 and VRK1.** *A,* GST-tagged VRK1 was pulled down with HeLa cell extracts. Eluted proteins were analyzed with SDS-PAGE and stained with Coomassie Brilliant Blue. MacroH2A1 was identified as a binding partner of VRK1 by MALDI-TOF. *B,* HEK293A cells were transfected with HA-macroH2A1, and cellular extract was pulled down with 10 μg of GST-VRK1. Each protein was detected by the indicated antibodies. *C,* recombinant proteins of His-macroH2A1 and GST-VRK1 were incubated and pulled down with GST-binding resins. 10 μg of GST-fused VRK1 was used, and variant amounts of macroH2A1 were applied. Each number means relative ratio to VRK1 protein. Separated by SDS-PAGE, each protein was detected by the indicated antibodies. *D,* HEK293A cells were transfected with HA-macroH2A1 and FLAG-VRK1, VRK2, and VRK3. Each set of cellular lysates was pulled down with anti-FLAG antibodies and analyzed with indicated antibodies. *E,* HeLa cells were transfected with red fluorescent protein-tagged VRK1 and FLAG-macroH2A1. After 24 h of expression, FLAG-macroH2A1 was visualized with specific antibody and Alexa 488-conjugated secondary antibody with fluorescence microscope. *IP*, immunoprecipitation; *IB*, immunoblot.

chromatin is inversely related to the level of macroH2A1. Because macroH2A1 specifically interacts with VRK1, we hypothesized that the mitotic Thr-3/Ser-10 phosphorylation of histone H3 by VRK1 occurs when the nucleosomal levels of macroH2A1 are lowered and that residual macroH2A1 might prevent VRK1 from phosphorylating histone H3 tails during interphase.

Ectopic MacroH2A1 Suppresses Mitotic Phosphorylation and Cell Cycle Progression—To better define the relationship between macroH2A1 and the mitotic index assessed by histone H3 phosphorylation, we tested whether ectopically expressed macroH2A1 can suppress the phosphorylation of histone H3. For this, HEK293A cells were transfected with enhanced green fluorescence protein (EGFP) alone or with EGFP-tagged macroH2A1 (EGFP-macroH2A1). After 24 h of expression, cells were harvested and analyzed to determine the phosphorylation of histone H3 at Ser-10 using flow cytometry (Fig. 3*A*). We first checked the transfection efficiency of our system (Fig. 3*A*, *top panel*) and analyzed the phosphorylation of Ser-10 of histone H3 in EGFP-positive cells. The amount of phospho-Ser-10 in histone H3 was markedly decreased in EGFP-macroH2A1-transfected cells compared with control cells (Fig. 3*A*, *bottom panel*). In addition, we found that high expression levels of macroH2A1 prevented cells from progressing into the mitotic phase (supplemental Fig. S3). This suggests that macroH2A1 may suppress the enzymatic action of VRK1, preventing normal cell cycle progression and stopping cells from reaching mitosis.

For a more detailed investigation into macroH2A1-mediated inhibition of VRK1 in cell proliferation, we measured the amount of incorporated bromodeoxyuridine (BrdU) in macroH2A1-transfected cells using flow cytometry (Fig. 3*B*). Cells were transfected with EGFP-macroH2A1 for 24 h, followed by a 1-h pulse of BrdU. For convenience, we divided quadrant plots according to the intensity of BrdU and EGFP signals and then analyzed ratios. EGFP-expressing cells were stained with BrdU to about 40%, whereas EGFP-macroH2A1-expressing cells were stained with BrdU to about 30%. Reduced populations of cycling cells may be induced due to macroH2A1-mediated G_2/M arrest. In particular, a population of cells emitting strong green fluorescence among EGFP-macroH2A1-expressing cells was hardly stained with BrdU, compared with EGFP-expressing cells. Based on this result, we hypothesized that the overexpression of EGFP-macroH2A1 exerts inhibitory effects on VRK1 and suppresses the progression of the cell cycle. The proportion of BrdU-incorporated proliferating cells among the population of cells expressing high levels of macroH2A1 is 0.19, which is relatively low compared with the corresponding ratio (0.47) among the population of cells expressing moderate levels of macroH2A1.

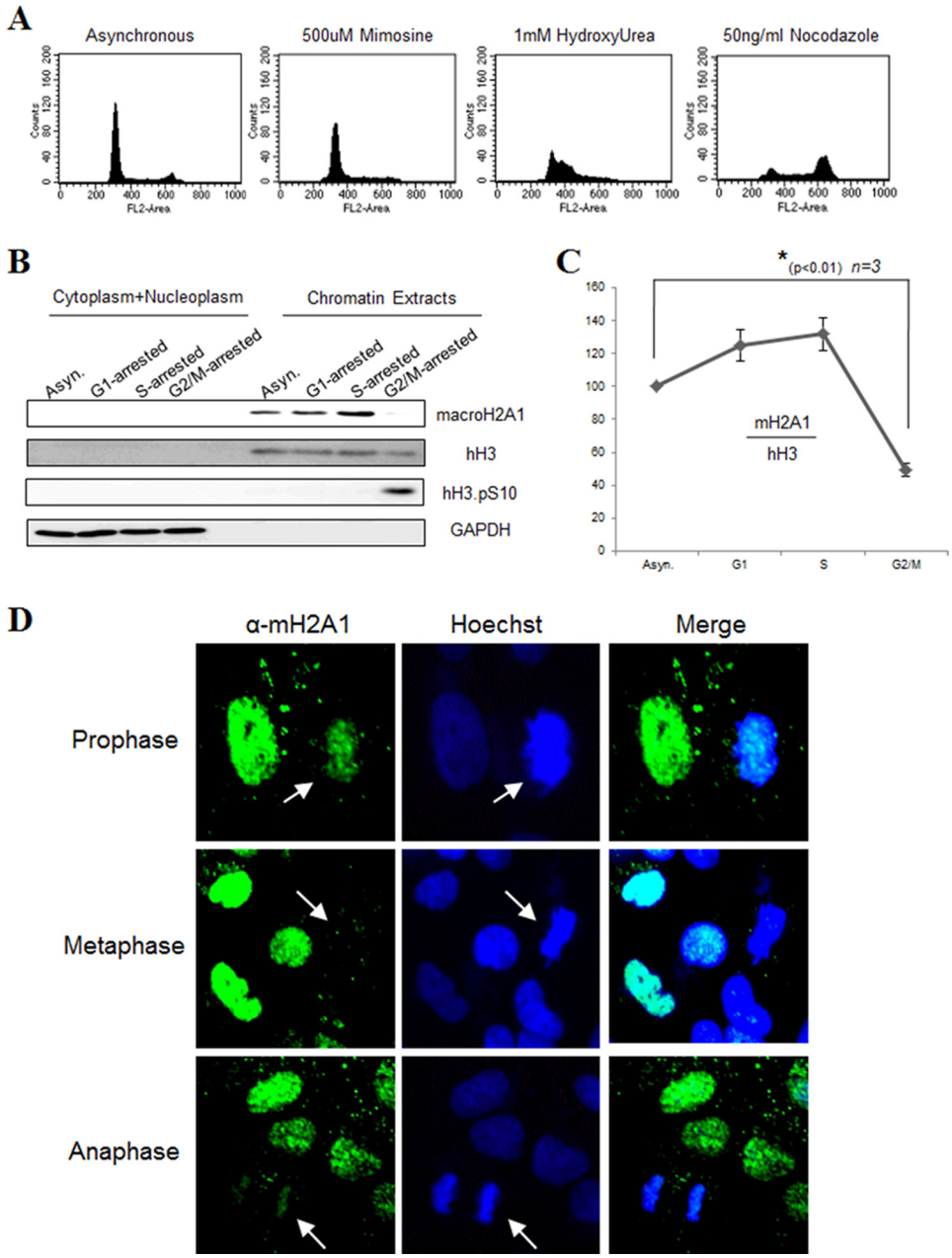

FIGURE 2. **Fluctuation of macroH2A1 levels during cell cycle.** *A,* A549 cells were arrested in G_1 phase with mimosine or in S phase with hydroxyurea or in M phase with nocodazole. Propidium iodide-stained DNA contents were analyzed for verification of cell cycle synchronization with flow cytometry. *B,* after cell lysis, the chromatin extract was prepared and nucleosomal concentration of macroH2A1 was determined by immunoblotting. GAPDH and histone H3 were used as loading controls. *C,* relative amount of macroH2A1 was plotted with respect to the amount of histone H3. The *error bars* represent the mean ± S.D. ($n = 3$). *Asterisk* denotes a statistically significant changes ($p < 0.01$). *D,* nucleosomal concentrations of macroH2A1 were determined with immunostaining of macroH2A1 in A549 cells. MacroH2A1 was visualized with specific antibody and Alexa 488-conjugated secondary antibody. *Arrow* indicates denoted particular mitotic phase and presents weakened fluorescence.

To acquire more evidence in support of our hypothesis, we used siRNA to knock down macroH2A1 to about 50% as determined by densitometry and analyzed changes in the DNA content (Fig. 3*C*). A marked increase in the G_2/M ratio was seen in macroH2A1 knockdown cells compared with control cells. As shown in Fig. 3*D*, knockdown of macroH2A1 also increased the level of phospho-histone H3, with phosphorylation specifically on Thr-3 and Ser-10. This might be because macroH2A1-mediated suppression of VRK1 was relieved, allowing VRK1 to phosphorylate more histones. To analyze the dependence of VRK1 toward histone H3 phosphorylation, macroH2A1 was knocked down concomitantly with the reduction of three major mitotic histone kinases, and the levels of phospho-histones were analyzed. Specific knockdown of macroH2A1 increased phosphorylation of histone H3 on Ser-10 and Thr-3 by 150 and 215%, respectively. However, knockdown of VRK1 significantly diminished the effect of the macroH2A1 RNAi. This indicates that the macroH2A1 RNAi-mediated increase of phospho-histones is mediated by VRK1. In particular, when we knocked down Aurora kinase B or haspin kinase in addition to the knockdown of macroH2A1, the levels of phospho-histones were higher, compared with those seen with knockdown of

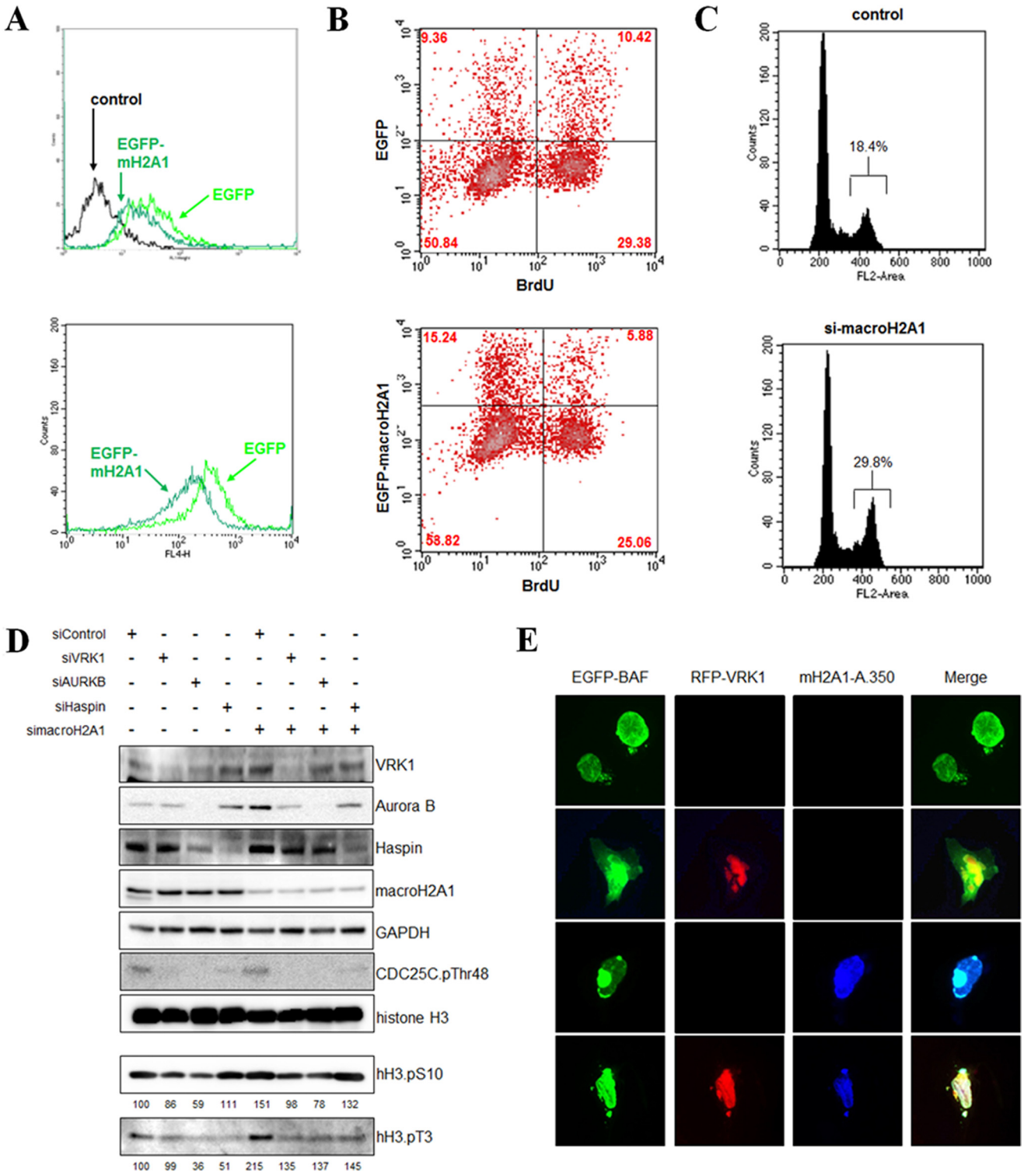

FIGURE 3. **Ectopic macroH2A1 suppresses mitotic phosphorylation and cell cycle progression.** *A,* HEK293A cells were transfected with EGFP or EGFP-macroH2A1. After 24 h of expression, cells were fixed and permeabilized with 95% of ethanol. Antibody against phospho-Ser-10 of histone H3 was incubated, and Alexa 596-conjugated secondary antibody was labeled for FACS analysis. Transfection efficiency was validated by analyzing amplitude of green fluorescence (*top panel*) and patterns of phospho-Ser-10 of histone H3 were analyzed (*bottom panel*). *B,* HEK293A cells were transfected with EGFP or EGFP-macroH2A1. Pulse labeling of transfected cells was performed with BrdU for 1 h. Allophycocyanin-conjugated anti-BrdU antibody was applied to fixed cells and analyzed by FACS. Allophycocyanin-BrdU-labeled EGFP-/EGFP-macroH2A1-transfected cells were analyzed in density plot, and quadrant statistics are presented at each corner. *C,* HEK293A cells were transfected with siRNA against macroH2A1. After 24 h of expression, cells were fixed and permeabilized with 95% ethanol. Flow cytometry was performed and propidium iodide-stained DNA content was visualized. *D,* A549 cells were transfected with specific siRNAs against macroH2A1, VRK1, Aurora kinase B, and haspin. After 36 h expression, 50 ng/ml nocodazole was treated for 12 h, and cells were harvested, and cellular lysates were extracted. Indicated proteins were analyzed by using specific antibodies. *E,* A549 cells were transfected with EGFP-BAF, DsRed1-monomer-VRK1, and FLAG-macroH2A1. After 24 h of expression, immunostaining was performed with FLAG antibody. FLAG-macroH2A1 was visualized by using Alexa 350-conjugated secondary antibody.

either Aurora kinase B or haspin kinase by RNAi. This suggests that Aurora kinase B and haspin kinase are not influenced by macroH2A1, but free VRK1 liberated from macroH2A1 phosphorylates more histones. The reason why phospho-histones are not elevated to control levels is because Aurora kinase B and haspin kinase seem to have a greater contribution to the phosphorylation of H3-Thr-3 and H3-Ser-10 than does VRK1. Considering these results together, we conclude that macroH2A1 suppresses the VRK1-dependent phosphorylation of H3-Thr-3 and H3-Ser-10. We also analyzed phosphorylation at Thr-48 of CDC25C, a well known marker for mitotic entry (29). Knockdown of macroH2A1 did not change the level of phosphorylation of CDC25C-Thr-48. These results suggest that the macroH2A1 RNAi-mediated increase in the population of cells containing 4N DNA is arrested in G_2 phase.

We further checked VRK1-mediated phosphorylation of other substrates in the presence of ectopically expressed macroH2A1 in mammalian cells. BAF is a well known substrate for VRK1 and is reported to be phosphorylated by VRK1 for proper cell cycling. This reaction triggers the nucleo-cytoplasmic shuttling of phosphorylated BAF (9). We analyzed changes in this well known physiological process upon ectopic expression of macroH2A1 (Fig. 3*E*). As reported previously (9), EGFP-BAF was localized in the nucleus by itself but was shuttled to the cytoplasm along with RFP-VRK1 in this assay. However, no efficient shuttling of BAF occurred when we expressed VRK1 along with macroH2A1. This suggests that ectopically expressed macroH2A1 interacts with VRK1 and suppresses its enzymatic action on BAF. These results indirectly support our assertion that macroH2A1 suppresses the catalytic activity of VRK1.

MacroH2A1 Suppresses the Activity of VRK1 but Not Other Histone Kinases—MacroH2A1 was pulled down with recombinant VRK1, and ectopic macroH2A1 expression resulted in several defects in VRK1-mediated physiological responses, as described above. We next analyzed the biochemical characteristics of macroH2A1 in the action of VRK1.

The histone domain of macroH2A1 has about 60% homology to histone H2A and is present in the nucleosome core particle along with histone H2B, substituting for the conventional H2A-H2B dimer (25). However, the macrodomain of macroH2A1 is exposed to the nucleoplasm and its biological roles are not well elucidated. As the exposed macrodomain of macroH2A1 might possibly interact with VRK1 in the nucleosome core particle, unlike its histone domain, we tested the effect of the macrodomain on VRK1. In contrast to full-length macroH2A1, the macrodomain effectively suppressed the catalytic activity of VRK1 (Fig. 4*A* and supplemental Fig. S4) in both its auto-phosphorylation and in the phosphorylation of its substrate histone H3 in the nucleosome core particle. To delineate the effect of macroH2A1 on VRK1, we synthesized an siRNA against macroH2A1 that targets the 3′-UTR. This siRNA targets endogenous macroH2A1 but not exogenously delivered macroH2A1. As presented in Fig. 4*B*, siRNA targeting the 3′-UTR of macroH2A1 increased the amount of phospho-histone H3, consistent with our previous findings. However, the ectopic expression of RNAi-resistant macroH2A1 rescued this phenotype. This suggests that macroH2A1 may affect mitotic histone H3 kinase activity. Interestingly, the macrodomain competed with histone H3 for VRK1 binding, as indicated by the fact that addition of increasing amounts of the macrodomain reduced the binding of histone H3 to VRK1 (Fig. 4*C*). These results indicate that the macrodomain of macroH2A1 can suppress the enzymatic activity of VRK1.

Next, we examined whether macroH2A1 affects the ability of VRK1 to phosphorylate other substrates such as BAF. As shown in Fig. 4*D*, the macrodomain at higher concentrations effectively inhibited the phosphorylating activity of VRK1 toward BAF, in addition to suppressing its auto-phosphorylation. Taken together, these data suggest that macroH2A1 interacts with VRK1 and affects its auto-phosphorylation as well as the phosphorylation of its substrates (histone H3 and BAF).

We have shown that macroH2A1 suppresses the enzymatic activity of VRK1 at Thr-3 and Ser-10 of histone H3. However, VRK1 is not the sole kinase involved in the phosphorylation of histone H3. Therefore, we tested whether macroH2A1 negatively regulates Aurora kinase B and haspin, which have been shown to phosphorylate Ser-10 and Thr-3 of histone H3, respectively (18, 19). As shown in Fig. 4*E*, ectopically expressed haspin markedly elevated the level of phospho-Thr-3 in histone H3. We also expressed macroH2A1 together with haspin and found that macroH2A1 did not induce any change in the level of phospho-Thr-3 in histone H3, suggesting that macroH2A1 did not inhibit haspin. We also examined the effect of macroH2A1 on Aurora kinase B. As shown in Fig. 4*F*, the level of phosphorylated Ser-10 increased slightly when Aurora kinase B was expressed in the presence of macroH2A1, even though we did not add inner centromere protein (INCENP), which is required for the full activity of Aurora kinase B (30). Taken together, these data lead to the conclusion that macroH2A1 exerts little inhibitory effect on the other mitotic histone kinases involved in the phosphorylation of Thr-3 and Ser-10 of histone H3.

Modeling the VRK1-Macrodomain Complex—The NMR structure of VRK1 was recently determined (31); therefore, we analyzed the nature of the interaction between VRK1 and macroH2A1. Two-dimensional ^{1}H-^{15}N heteronuclear single quantum correlation (HSQC) spectroscopy was used to examine the molecular interaction between ^{15}N-labeled VRK1 and the unlabeled macrodomain. As shown in Fig. 5, *A* and *B*, a number of VRK1 residues showed chemical shift perturbations in the HSQC spectrum upon the addition of the macrodomain, indicating that the macrodomain interacts with VRK1. NMR chemical shift mapping data were utilized to generate ambiguous interactive restraints, which were then input into the program HADDOCK to develop a protein-protein interaction model of VRK1 and macroH2A1 (Fig. 5, *A* and *B*).

The crystal structure of human macroH2A1 (Protein Data Bank code 1ZR5) was used to develop a docking model. The residues on VRK1 that show chemical shift changes when the macro histone binds, and are also solvent-exposed in the three-dimensional structure, were defined as active residues as follows: Lys-179, Gly-223, Thr-224, Lys-350, Lys-352, Thr-353, Thr-355, and Lys-356. The web server WHISCY was utilized to confirm the active residues of VRK1 and predict the active residues of the macrodomain of macroH2A1. The lowest energy

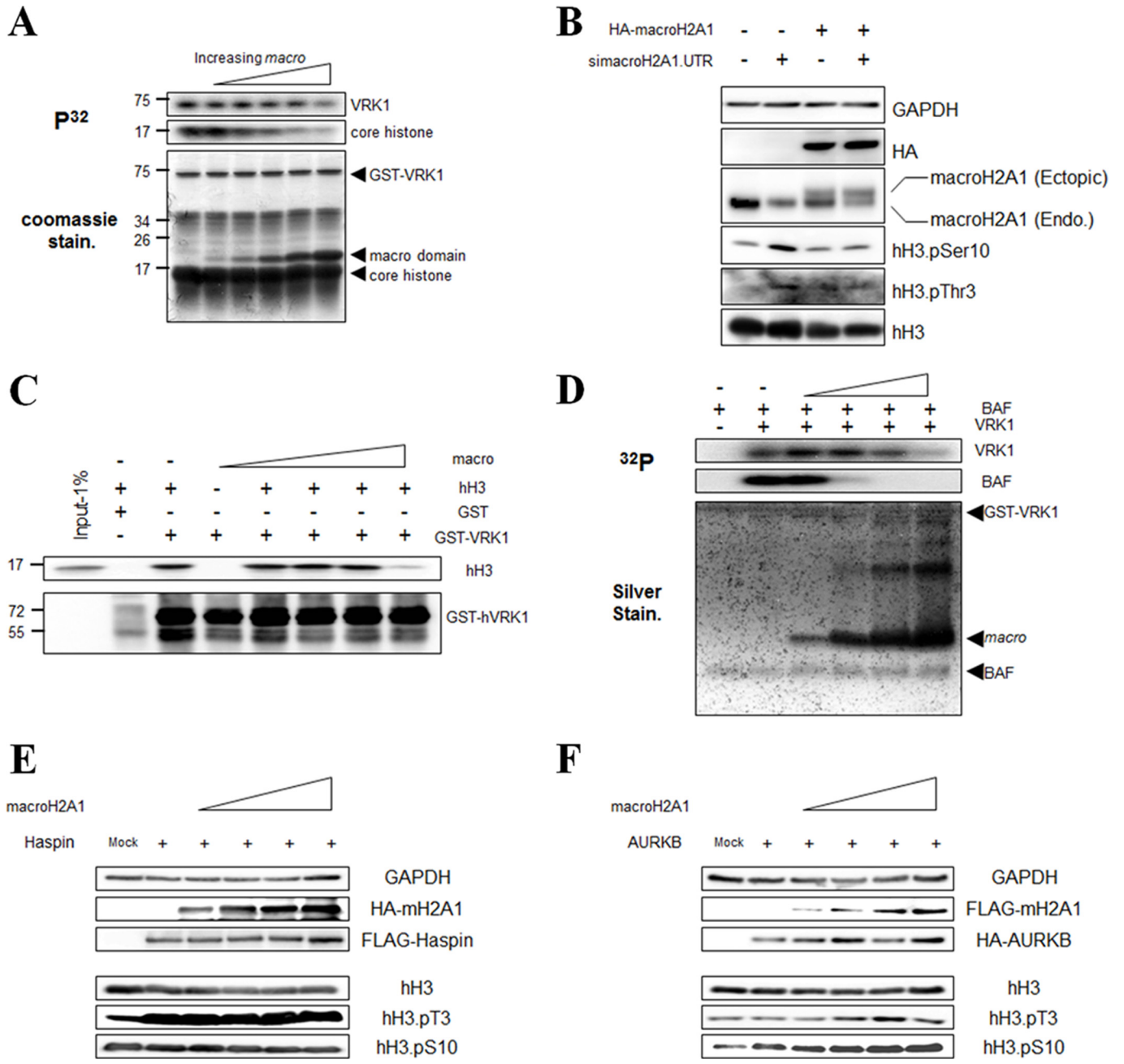

FIGURE 4. **MacroH2A1 suppresses the activity of VRK1 but not other histone kinases.** *A, in vitro* kinase assay was performed with recombinant GST-VRK1 and macrodomain. Core histone complex was used as a substrate of VRK1. Autoradiograph was acquired, and the gel was stained with Coomassie Brilliant Blue. *B,* A549 cells were transfected with HA-macroH2A1 and siRNA against 3′-UTR of endogenous (*Endo*) macroH2A1. After 24 h of expression, total lysates were analyzed by immunoblotting. GAPDH and histone H3 were visualized as loading controls. *C,* competitive inhibition by macrodomain against binding between VRK1 and histone H3 was determined by using recombinant GST-VRK1, macrodomain, and core histone complex. GST-VRK1 was pulled down, and each protein was immunoblotted by using specific antibodies. *D, in vitro* kinase assay was performed with recombinant GST-VRK1 and macrodomain. Recombinant BAF protein was used as a substrate of VRK1. Autoradiograph was acquired, and then gel was stained with Coomassie Brilliant Blue. *E* and *F,* HEK293T cells were transfected with indicated plasmids. After 24 h of expression, cells were harvested; cellular lysates were extracted, and phospho-histone H3 was analyzed by using specific antibodies. GAPDH and histone H3 were used as loading controls.

structure from the lowest energy cluster of models is shown in Fig. 5*C*. A preponderance of hydrophilic and hydrophobic interactions was observed between the C-terminal region (349–357) of VRK1 and the C-terminal end of the macrodomain (352′–358′). The VRK1 catalytic loop formed by residue Ser-181 shows hydrogen bonding interactions with Ser-354 in the binding partner. Our model predicts that residue Glu-355 of the macrodomain can form several hydrogen bonds with Lys-352, Thr-353, and Thr-355 of VRK1 (Fig. 5*D*). Several hydrophobic interactions are also predicted to be located at the binding interface between VRK1 and macroH2A1. Taken together, our NMR chemical shift data suggest that the macrodomain directly interacts with certain critical residues in the core catalytic domain as well as in the C-terminal tail of VRK1, thereby inhibiting its activity. We have therefore evaluated these protein-protein docking predictions by engineering

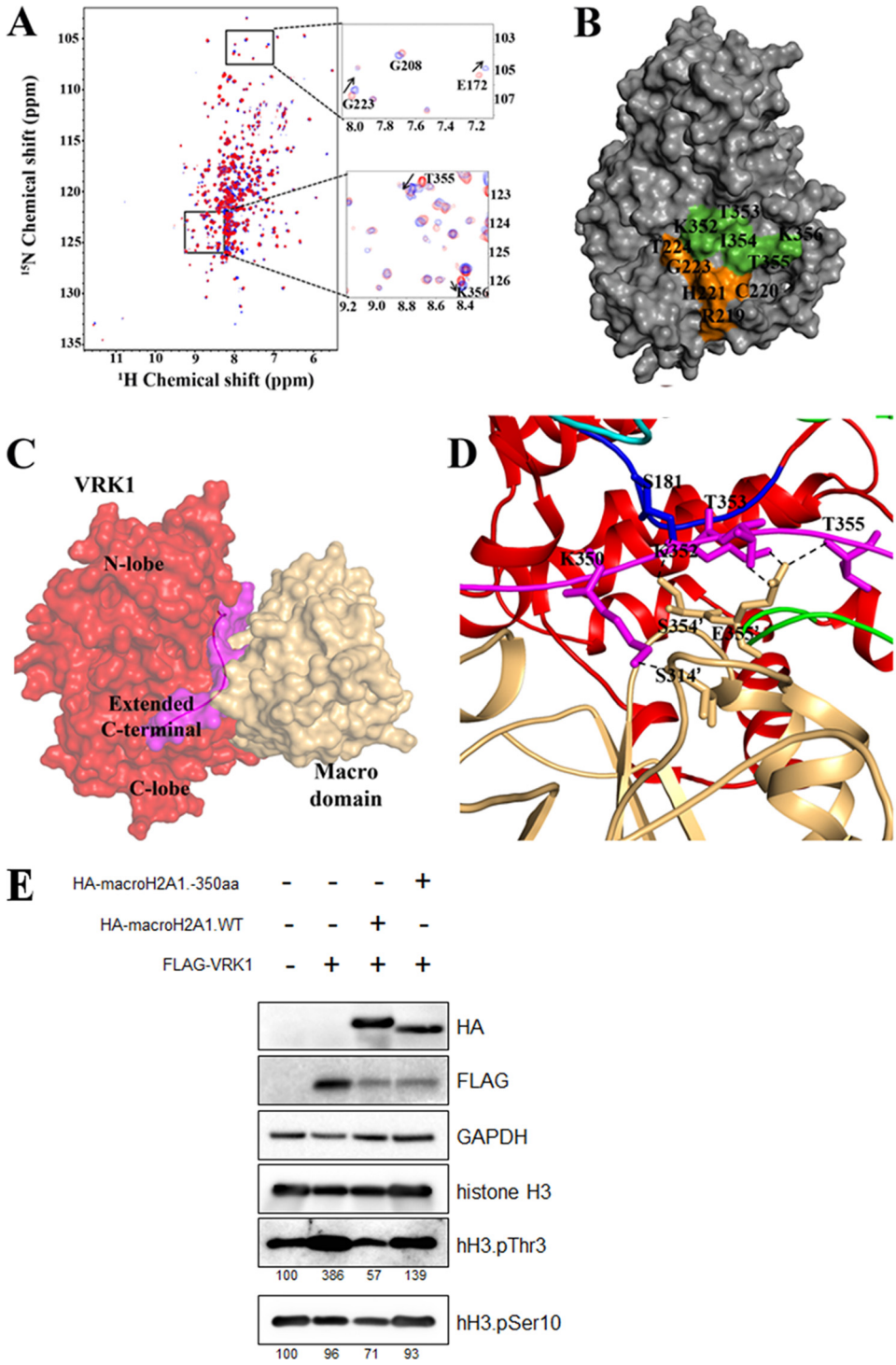

FIGURE 5. **Modeling the VRK1-macrodomain complex.** *A,* overlay of ^{1}H-^{15}N TROSY-HSQC spectra of 0.1 mM ^{15}N-labeled VRK1 alone (*red*) and in the presence of 0.5 mM unlabeled macrodomain of macroH2A1 (*blue*). The positions of peaks in the catalytic/activation loops and C-terminal extension of VRK1 affected by interaction with macroH2A1 are shown on the *right side of panel* as expanded sections. *B,* binding site mapping between macrodomain macroH2A1 and VRK1 on the surface of VRK1 structure based on the NMR titration experiments. Residues of VRK1 affected by the interaction are displayed in *green* (C-terminal extension) and *orange* (activation loop), respectively. *C,* binding mode of macrodomain with VRK1 was highlighted with surface view, and the C-terminal part of VRK1 is highlighted with *magenta*. *D,* residues from all the important regions like G-loop (*cyan*), catalytic loop (*blue*), activation loop (*green*), and C-terminal region (*magenta*) are involved in macrodomain binding. Majority of interactions are observed with C-terminal residues (Lys-350, Lys-352, Thr-353 and Thr-355). *E,* A549 cells were transfected with wild-type HA-macroH2A1 or C-terminal truncated form of HA-macroH2A1 that ends at the 350th amino acid. FLAG-VRK1 was cotransfected. phospho-histone H3 was analyzed by using specific antibodies.

three-point mutations on macroH2A1; these mutants demonstrated lower inhibition than did the wild-type protein (supplemental Fig. S5).

Based on our NMR titration analysis, we propose that macroH2A1 binds VRK1 via its C-terminal end (amino acids 351–357). Thus, we further generated a C-terminal truncated

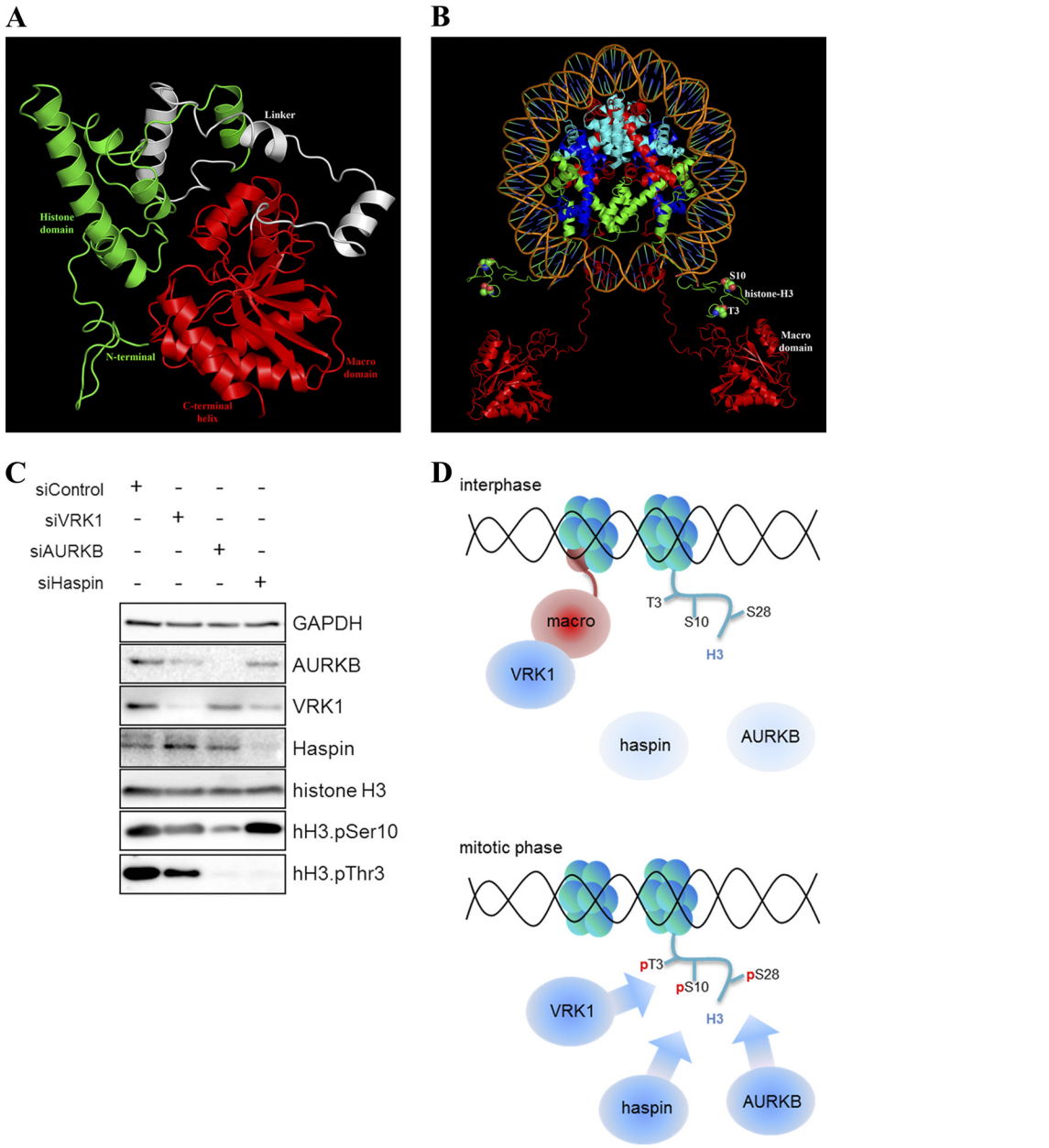

FIGURE 6. **Experimental models.** *A,* homology models were developed for full-length macroH2A1 to elucidate the possible reasons for binding ability differences with VRK1 by full-length macroH2A1 and macrodomain alone. I-TASSER three-dimensional protein prediction server was utilized to develop the homology models. The server utilized Protein Data Bank code 2F8N coordinates to build the histone domain and 2FXK for the macrodomain. The flexible linker that connects the histone and macrodomain was built by *ab initio* modeling by the I-TASSER. All the five models derived from the predictions revealed that the histone domain orients close to the macrodomain and masks the macrodomain and may hinder the interaction of VRK1 and the macrodomain. The N-terminal histone domain is highlighted in *green*, flexible linker in *white,* and macrodomain shown in *red*. *B,* theoretical model of nucleosome core particle was developed by utilizing the several existing crystal structures as well as incorporating the molecular model of macroH2A1 based on existing data. X-ray crystal structure of the nucleosome core particle (Protein Data Bank code 1KX5) was utilized to develop the model as this crystal structure consisted of the full-length histone H3 and relatively long histone H2A (consists of 128 resides unlike other structures having around 120). This three-dimensional structure facilitates the relative orientation of histone H2A and histone H3 domains in nucleosome core particle complex. This structure reveals the terminal ends (N-terminal end of H3 and C-terminal end of histone H2A) of these two domains are in close proximity. The macroH2A structure, which is the variant of histone H2A, was acquired from the 2F8N crystal structure and the histone H2A in 1KX5 is replaced with macroH2A. The linker part with the macrodomain of macroH2A1 is connected to macrohistone H2A (2F8N) by molecular modeling tools incorporated in InsightII modules. Our hypothetical model gives an idea that VRK1 interacts with the H3 N-terminal end and phosphorylates the Thr-3 and Ser-10 residues when histone H2A is presents in the nucleosome core particle. In the interphase of the cell cycle, macroH2A1 (variant of histone H2A) occupies the histone H2A position and competes with the H3 for VRK1 binding. Because of the presence of the macrodomain, macroH2A1 may provide an extra surface for VRK1 binding, and VRK1 may prefer the macroH2A1. The linker region that connects the histone and macrodomain may also play a crucial role for flexibility of two domains and interfering with VRK1 and H3 interaction. *C,* relative contribution of VRK1 to histone H3 phosphorylation was analyzed by comparing it with haspin kinase and Aurora kinase B. A549 cells were transfected with siRNAs against VRK1, Aurora kinase B, and haspin. Indicated proteins were analyzed by using specific antibodies. *D,* schematic model suggesting interphase-specific suppression of VRK1 by macroH2A1. At interphase, macroH2A1-dependent inhibition of VRK1 and low expression level of Aurora kinase B/haspin make no phosphorylated histone H3. However, at mitotic phase three kinds of fully active mitotic kinases cause extensive phosphorylation on tails of histone H3.

form of macroH2A1 that ends at residue 350 (hereafter called macroH2A1–350aa). As shown in the Fig. 5*E*, ectopic expression of wild-type macroH2A1 decreased the level of phosphorylation of Thr-3 and Ser-10 on histone H3. However, the putative unbound form of macroH2A1 (macroH2A1–350aa) did not reduce the levels of phospho-histones. These results demonstrate the cellular consequences of the interaction between macroH2A1 and VRK1, and the nature of the interaction between the two proteins.

DISCUSSION

VRK1 is a novel Ser/Thr kinase that is expressed constantly during interphase, and it appears to play an important role during this period in the cell cycle (13, 14, 20). However, VRK1-mediated phosphorylation of histone H3 needs to be restricted until the time of transition from the late G_2 phase to the mitotic phase (18, 19). This event is tightly regulated because unregulated phosphorylation of histones triggers chaotic cellular responses (18).

The present studies suggest that macroH2A1 serves as a possible candidate for a negative regulator of VRK1 activity during interphase. This was validated by our *in vitro* assays using the macrodomain of macroH2A1. The macrodomain effectively blocked the interaction between histone H3 and VRK1 and also inhibited the phosphorylation of VRK1 substrates, including histone H3 and BAF. We performed an *in vitro* kinase assay with increasing amounts of full-length macroH2A1, which showed that macroH2A1 had relatively little effect on the auto-phosphorylation of VRK1 even when a 10-fold molar excess of macroH2A1 was added to VRK1. Full-length macroH2A1 was not very effective in inhibiting VRK1 auto-phosphorylation, even though it inhibited the phosphorylation of histone H3. This might be attributable to the difference between purified free macroH2A1 and cellular macroH2A1 in the nucleosome. As predicted in our homology model (Fig. 6*A*), in the free macroH2A1 conformation, the histone domain may be oriented close to the macrodomain, masking the macrodomain and consequently hindering the interaction of the macrodomain with VRK1. However, in the macroH2A1-charged nucleosome *in vivo*, as shown in a modeled nucleosome core particle with full-length H3 and macroH2A1 (Fig. 6*B*), the macrodomain may be exposed, allowing macroH2A1 to favorably interact with VRK1 and subsequently affecting the VRK1-mediated phosphorylation of histone H3 in the nucleosome.

It is known that the function of macroH2A1 is related to the X chromosome inactivation (23, 26, 27). Apart from its function as an X chromosome silencer, macroH2A1 has also been reported to prevent transcription factors from interacting with promoter/enhancer regions (24, 25). However, its physiological role in the cell cycle currently remains unknown. Our present results indicate that macroH2A1 is a novel binding partner of VRK1 and suppresses its enzymatic activity during interphase. This mode of suppression by macroH2A1 appears to be maintained during interphase. However, in the mitotic phase, the protein level of macroH2A1 decreases; VRK1 is liberated, and its activity is potentiated.

Additionally, we further analyzed the relative contribution of VRK1 to histone H3 phosphorylation by comparing it with haspin kinase and Aurora kinase B (Fig. 6*C*). Our results indicate that VRK1 also plays a role in mitotic phosphorylation of histone H3; however, it seems to be less potent than Aurora kinase B and haspin. Aurora kinase B directly phosphorylates H3-Ser-10 and also indirectly affects phosphorylation of H3-Thr-3 by regulating haspin (21).

Based on our results, we propose a model summarizing our experimental results (Fig. 6*D*). However, our model of the macroH2A1-mediated regulation of VRK1 is not complete and cannot completely explain all physiological conditions. The nucleosomal level of macroH2A1 did not appear to be enough to substitute for H2A in an all-or-none manner. The amount of macroH2A1 was maintained during the mitotic phase even though its level was less than 50% of that seen in interphase. The results of our *in vitro* enzyme assay suggest that small amounts of macroH2A1 can effectively suppress the enzymatic activity of VRK1. Thus, we cannot exclude the possibility that other nuclear factors may neutralize the inhibitory action of macroH2A1 on VRK1. A recent report showed that the hinge region of macroH2A1 can be phosphorylated by cyclin-dependent kinases (27). This may contribute to the inhibition of macroH2A1 in nucleosomes during mitosis if phospho-macroH2A1 loses its suppressing activity against VRK1 and allows histone H3 to be phosphorylated by VRK1. The detailed mechanism of VRK1-mediated histone H3 phosphorylation in the cell cycle awaits further study addressing the orchestrated action of many other factors involved in this complex epigenetic regulation.

REFERENCES

1. Nichols, R. J., and Traktman, P. (2004) Characterization of three paralogous members of the mammalian vaccinia-related kinase family. *J. Biol. Chem.* **279,** 7934–7946
2. Lopez-Borges, S., and Lazo, P. A. (2000) The human vaccinia-related kinase 1 (VRK1) phosphorylates threonine 18 within the mdm-2-binding site of the p53 tumor suppressor protein. *Oncogene* **19,** 3656–3664
3. Barcia, R., López-Borges, S., Vega, F. M., and Lazo, P. A. (2002) Kinetic properties of p53 phosphorylation by the human vaccinia-related kinase 1. *Arch. Biochem. Biophys.* **399,** 1–5
4. Vega, F. M., Sevilla, A., and Lazo, P. A. (2004) p53 stabilization and accumulation induced by human vaccinia-related kinase 1. *Mol. Cell. Biol.* **24,** 10366–10380
5. Valbuena, A., Vega, F. M., Blanco, S., and Lazo, P. A. (2006) p53 down-regulates its activating vaccinia-related kinase 1, forming a new autoregulatory loop. *Mol. Cell. Biol.* **26,** 4782–4793
6. Valbuena, A., Castro-Obregón, S., and Lazo, P. A. (2011) Down-regulation of VRK1 by p53 in response to DNA damage is mediated by the autophagic pathway. *PLoS One* **6,** e17320
7. Sevilla, A., Santos, C. R., Barcia, R., Vega, F. M., and Lazo, P. A. (2004) c-Jun phosphorylation by the human vaccinia-related kinase 1 (VRK1) and its cooperation with the N-terminal kinase of c-Jun (JNK). *Oncogene* **23,** 8950–8958
8. Sevilla, A., Santos, C. R., Vega, F. M., and Lazo, P. A. (2004) Human vaccinia-related kinase 1 (VRK1) activates the ATF2 transcriptional activity by novel phosphorylation on Thr-73 and Ser-62 and cooperates with JNK. *J. Biol. Chem.* **279,** 27458–27465
9. Nichols, R. J., Wiebe, M. S., and Traktman, P. (2006) The vaccinia-related kinases phosphorylate the N terminus of BAF, regulating its interaction with DNA and its retention in the nucleus. *Mol. Biol. Cell* **17,** 2451–2464
10. Lancaster, O. M., Cullen, C. F., and Ohkura, H. (2007) NHK-1 phosphorylates BAF to allow karyosome formation in the *Drosophila* oocyte nucleus. *J. Cell Biol.* **179,** 817–824
11. Gorjánácz, M., Klerkx, E. P., Galy, V., Santarella, R., López-Iglesias, C.,

Askjaer, P., and Mattaj, I. W. (2007) *Caenorhabditis elegans* BAF-1 and its kinase VRK-1 participate directly in post-mitotic nuclear envelope assembly. *EMBO J.* **26,** 132–143
12. Santos, C. R., Rodríguez-Pinilla, M., Vega, F. M., Rodríguez-Peralto, J. L., Blanco, S., Sevilla, A., Valbuena, A., Hernández, T., van Wijnen, A. J., Li, F., de Alava, E., Sánchez-Céspedes, M., and Lazo, P. A. (2006) VRK1 signaling pathway in the context of the proliferation phenotype in head and neck squamous cell carcinoma. *Mol. Cancer Res.* **4,** 177–185
13. Kang, T. H., Park, D. Y., Kim, W., and Kim, K. T. (2008) VRK1 phosphorylates CREB and mediates CCND1 expression. *J. Cell Sci.* **121,** 3035–3041
14. Valbuena, A., López-Sánchez, I., and Lazo, P. A. (2008) Human VRK1 is an early response gene, and its loss causes a block in cell cycle progression. *PLoS One* **3,** e1642
15. Schober, C. S., Aydiner, F., Booth, C. J., Seli, E., and Reinke, V. (2011) The kinase VRK1 is required for normal meiotic progression in mammalian oogenesis. *Mech. Dev.* **128,** 178–190
16. Choi, Y. H., Park, C. H., Kim, W., Ling, H., Kang, A., Chang, M. W., Im, S. K., Jeong, H. W., Kong, Y. Y., and Kim, K. T. (2010) Vaccinia-related kinase 1 is required for the maintenance of undifferentiated spermatogonia in mouse male germ cells. *PLoS One* **5,** e15254
17. Wiebe, M. S., Nichols, R. J., Molitor, T. P., Lindgren, J. K., and Traktman, P. (2010) Mice deficient in the serine/threonine protein kinase VRK1 are infertile due to a progressive loss of spermatogonia. *Biol. Reprod.* **82,** 182–193
18. Dai, J., Sultan, S., Taylor, S. S., and Higgins, J. M. (2005) The kinase haspin is required for mitotic histone H3 Thr-3 phosphorylation and normal metaphase chromosome alignment. *Genes Dev.* **19,** 472–488
19. Crosio, C., Fimia, G. M., Loury, R., Kimura, M., Okano, Y., Zhou, H., Sen, S., Allis, C. D., and Sassone-Corsi, P. (2002) Mitotic phosphorylation of histone H. Spatio-temporal regulation by mammalian Aurora kinases. *Mol. Cell. Biol.* **22,** 874–885
20. Kang, T. H., Park, D. Y., Choi, Y. H., Kim, K. J., Yoon, H. S., and Kim, K. T. (2007) Mitotic histone H3 phosphorylation by vaccinia-related kinase 1 in mammalian cells. *Mol. Cell. Biol.* **27,** 8533–8546
21. Wang, F., Ulyanova, N. P., van der Waal, M. S., Patnaik, D., Lens, S. M., and Higgins, J. M. (2011) A positive feedback loop involving Haspin and Aurora B promotes CPC accumulation at centromeres in mitosis. *Curr. Biol.* **21,** 1061–1069
22. Pehrson, J. R., and Fried, V. A. (1992) MacroH2A, a core histone containing a large nonhistone region. *Science* **257,** 1398–1400
23. Costanzi, C., and Pehrson, J. R. (1998) Histone macroH2A1 is concentrated in the inactive X chromosome of female mammals. *Nature* **393,** 599–601
24. Agelopoulos, M., and Thanos, D. (2006) Epigenetic determination of a cell-specific gene expression program by ATF-2 and the histone variant macroH2A. *EMBO J.* **25,** 4843–4853
25. Angelov, D., Molla, A., Perche, P. Y., Hans, F., Côté, J., Khochbin, S., Bouvet, P., and Dimitrov, S. (2003) The histone variant macroH2A interferes with transcription factor binding and SWI/SNF nucleosome remodeling. *Mol. Cell* **11,** 1033–1041
26. Chadwick, B. P., and Willard, H. F. (2002) Cell cycle-dependent localization of macroH2A in chromatin of the inactive X chromosome. *J. Cell Biol.* **157,** 1113–1123
27. Bernstein, E., Muratore-Schroeder, T. L., Diaz, R. L., Chow, J. C., Changolkar, L. N., Shabanowitz, J., Heard, E., Pehrson, J. R., Hunt, D. F., and Allis, C. D. (2008) A phosphorylated subpopulation of the histone variant macroH2A1 is excluded from the inactive X chromosome and enriched during mitosis. *Proc. Natl. Acad. Sci. U.S.A.* **105,** 1533–1538
28. Park, C. H., Choi, B. H., Jeong, M. W., Kim, S., Kim, W., Song, Y. S., and Kim, K. T. (2011) Protein kinase Cδ regulates vaccinia-related kinase 1 in DNA damage-induced apoptosis. *Mol. Biol. Cell* **22,** 1398–1408
29. Kohn, E. A., Ruth, N. D., Brown, M. K., Livingstone, M., and Eastman, A. (2002) Abrogation of the S phase DNA damage checkpoint results in S phase progression or premature mitosis depending on the concentration of 7-hydroxystaurosporine and the kinetics of Cdc25C activation. *J. Biol. Chem.* **277,** 26553–26564
30. Vader, G., and Lens, S. M. (2008) The Aurora kinase family in cell division and cancer. *Biochim. Biophys. Acta* **1786,** 60–72
31. Shin, J., Chakraborty, G., Bharatham, N., Kang, C., Tochio, N., Koshiba, S., Kigawa, T., Kim, W., Kim, K. T., and Yoon, H. S. (2011) NMR solution structure of human vaccinia-related kinase 1 (VRK1) reveals the C-terminal tail essential for its structural stability and autocatalytic activity. *J. Biol. Chem.* **286,** 22131–22138